Article:

Magee, C orcid.org/0000-0001-9836-2365, Jackson, CA-L, Hardman, JP et al. (1 more author) (2017) Decoding sill emplacement and forced fold growth in the Exmouth Sub-basin, offshore northwest Australia: Implications for hydrocarbon exploration. Interpretation, 5 (3). SK11-SK22. ISSN 2324-8858

https://doi.org/10.1190/INT-2016-0133.1

Decoding sill emplacement and forced fold growth in the Exmouth Sub-basin, offshore NW Australia: implications for hydrocarbon exploration

Craig Magee[1], Christopher A-L Jackson[1], Jonathon P Hardman[2], Matthew T Reeve[1]

[1]Basins Research Group, Department of Earth Science and Engineering, Imperial College, Prince Consort Road, UK (c.magee@imperial.ac.uk; c.jackson@imperial.ac.uk; matthew.reeve09@imperial.ac.uk)

[2]Geology and Petroleum Geology, School of Geoscience, University of Aberdeen, Aberdeen, UK (jonathon.hardman@abdn.ac.uk)

Original paper date of submission: 12/08/2016

Revised paper date of submission: 22/11/2016

ABSTRACT

Igneous sills emplaced at shallow-levels in sedimentary basins commonly uplift the overburden and free surface. Uplift produces dome-shaped forced folds that may host economic hydrocarbon accumulations. These intrusion-induced forced folds are typically assumed to develop instantaneously, whereby the oldest onlapping strata constrain the age of sill emplacement, and accommodate the entire volume of intruded magma. However, several studies demonstrate that forced folds may grow over geological timescales, with additional space-making mechanisms (e.g., compaction) partly accommodating the magma volume. It is thus critical to understand when forced fold traps form and how they evolve in relation to the timing of source rock maturation and migration. We analyze two forced folds imaged in 2D seismic reflection data from offshore NW Australia. Analyzing the seismic stratigraphy of the forced fold overburden allows us to recognize several distinct phases of fold growth. Sub-horizontal reflections onlapping onto the lower portion of the forced folds at a high angle indicate that the first phase of sill emplacement and fold development occurred rapidly, facilitated by normal faulting, prior to deposition of overlying strata during a period of magmatic quiescence and regional hydrocarbon maturation in the Early Cretaceous. Renewed magmatic activity resulted in a final, protracted phase of doming, which is recorded by a package of onlapping growth strata that was incrementally deformed by successive intrusive pulses. We also demonstrate that in addition to folding and faulting, the magma volume was likely accommodated by porosity within the folded strata. Our observations imply that the age of the lowermost onlapping reflections only constrain the onset of sill emplacement and not the duration of magmatic activity. Constraining the dynamic evolution of intrusion-induced forced folds from the structure of onlapping reflections during hydrocarbon exploration can thus provide critical insights into the potential volume and charge history of any hydrocarbon accumulations.

INTRODUCTION

The shallow-level emplacement of igneous sills and laccoliths in sedimentary basins is commonly accommodated by uplift and folding of overlying strata and the free surface (Fig. 1A) (e.g., Johnson and Pollard, 1973; Pollard and Johnson, 1973; Hansen and Cartwright, 2006; Galland, 2012; Jackson et al., 2013; Magee et al., 2013a; Agirrezabala, 2015). Because uplift occurs directly above and as a result of the injection and inflation of sill intrusions, these types of folds are termed ‘forced folds’ (Stearns, 1978; Trude et al., 2003; Hansen and Cartwright, 2006). Sill-related forced folds are typically dome-shaped morphologies (i.e. four-way dip closures), broadly mirroring the geometry of the underlying intrusion(s), and may thus represent potential hydrocarbon traps (Fig. 1B) (Schutter, 2003; Hansen and Cartwright, 2006; Polteau et al., 2008; Holford et al., 2012; Jackson et al., 2013). For example, sills and laccoliths in the Neuquén Basin, Argentina have locally matured shales that source oil accumulations (20–33° API) in overlying forced folds (e.g., Fig. 1B) (Rodriguez Monreal et al., 2009). Whilst the overarching geometry of intrusion-induced forced folds makes them attractive exploration targets (Fig. 1B), syn-kinematic deformation (e.g., compaction and faulting) and diagenetic alteration (e.g., by contact metamorphism) of the folded strata can promote or inhibit the migration and/or accumulation of hydrocarbons (Holford et al., 2012). To de-risk exploration associated with and understand intrusion-induced forced folds, it is therefore critical to evaluate the dynamic evolution of forced folds.

Determining the processes driving and accompanying intrusion-induced forced fold formation requires the analysis of deformed strata above ancient sills and/or laccoliths, either exposed at the Earth's surface or imaged in seismic reflection data (e.g., Hansen and Cartwright, 2006; Jackson et al., 2013; Magee et al., 2013a; Magee et al., 2014; Agirrezabala, 2015; Wilson et al., 2016). Three-dimensional seismic reflection data in particular have revolutionized our understanding of forced fold growth and sill emplacement, highlighting that: (1) intrusion geometry and the behavior of the host rock during deformation dictate forced fold morphology (e.g., Jackson et al., 2013; Magee et al., 2013a); (2) onlap of overlying reflections onto folded strata can be used to absolutely or relatively date forced folding (Trude et al., 2003); and (3) sill intrusion and forced fold growth within sedimentary basins may be incremental and protracted (i.e. occur over several million years), and not geologically instantaneous (Magee et al., 2014). Although intrusion-induced forced folds may be expressed at the paleosurface for a considerable period of time, very few studies have considered how onlap patterns in the overlying strata may be used to unravel fold evolution (Magee et al., 2014).

Here, we use time-migrated 2D seismic reflection data to examine the evolution of forced folds developed above multiple sills located offshore NW Australia in the Exmouth Sub-basin (Fig. 2). In particular, we show how onlap patterns in overlying strata allow us to determine the overall timing of magmatic activity and the detailed kinematics of fold growth. Our results reveal that two forced folds formed to accommodate the emplacement of multiple, stacked and overlapping sills during the Upper Jurassic, prior to the onset of regional hydrocarbon generation and migration in the Early Cretaceous (Tindale et al., 1998). Vertical variations in the degree of folding and dip of overlying strata suggest that the folds developed in two distinct phases over a protracted time-span, likely in response to incremental magma injection; i.e. the fold did not form instantaneously. During doming, outer-arc extension across the fold crest promoted the development of intra-fold normal faults (e.g., Pollard and Johnson, 1973; Magee et al., 2013a). We also argue that a concurrent reduction in porosity of the host rock, due to fluidization and/or compaction, partly accommodated the emplaced magma volume (e.g., Schofield et al., 2012; Magee et al., 2013a). Whilst the forced folds may have formed suitable traps for hydrocarbons in the Early Cretaceous, due to a lack of borehole data we are unable to directly quantify the impact of outer-arc extension faults and host rock porosity reduction on migration pathways, reservoir quality, and structure compartmentalization. Importantly, however, we are able to show that: (1) forced folds expressed at the surface can influence sediment routing and deposition for protracted time-spans; (2) the architecture of onlapping strata can be used to assess fold evolution; and (3) the age of the lowermost reflections that onlap onto the fold can only be used to date the onset of sill emplacement and not necessarily the duration of magmatic activity as assumed by many previous studies (e.g., Trude et al., 2003; Hansen and Cartwright, 2006; Jackson et al., 2013; Magee et al., 2013a).

GEOLOGIC SETTING

The Exmouth Sub-basin, which forms part of the North Carnarvon Basin (Figs 2A and B), formed in response to Early Jurassic and Late Jurassic-to-Early Cretaceous rifting between Greater India and Australia (Fig. 3) (e.g., Stagg and Colwell, 1994; Tindale et al., 1998; Longley et al., 2002). Here, we focus on the Northern and Central elements of the Exmouth Sub-basin, which contain thick (up to 3.5 km) Jurassic sequences and are separated from the Carnarvon Terrace element to the south by the Ningaloo Arch (Fig. 2); little to no Jurassic strata was deposited and/or is preserved across the Ningaloo Arch and Carnarvon Terrace (Mihut and Müller, 1998; Tindale et al., 1998; Müller et al., 2002). Across the Exmouth Plateau to the north, the Jurassic sequence is either absent or condensed (Exon et al., 1992; Stagg and Colwell, 1994).

Pre-rift strata within the Northern Exmouth Sub-basin primarily comprises a thick section of the Upper Triassic, fluvio-deltaic to marginal marine Mungaroo Formation, which is overlain by the marine Murat Siltstone (Fig. 3) (Hocking et al., 1987; Tindale et al., 1998). During the first rift phase in the Early Jurassic, NE-striking, large-displacement (up to 1 km) normal faults developed and syn-rift sequences of the Athol and Calypso formations, which together are up to 1.5 km thick, were deposited (Figs 3 and 4) (Hocking, 1992; Tindale et al., 1998; Longley et al., 2002). The Late Jurassic-to-Early Cretaceous rift phase produced a dense array of NW- to NE-striking, low-displacement (*c*. <0.1 km) normal faults within the 2 km thick, Oxfordian-to-Tithonian, marine shale-dominated Dingo Claystone (Figs 3 and 4) (e.g., Hocking, 1992; Tindale et al., 1998; Magee et al., 2016a). Where present, the sand-rich

Dupuy Formation is laterally equivalent to the upper portion of the Dingo Claystone (Ross and Vail, 1994; Reeve et al., 2016). Towards the northern margin of the Northern and Central Exmouth Sub-basins, the Tithonian-to-Valanginian, deltaic Barrow Group overlies the Dingo Claystone and, in places, the Dupuy Formation (Fig. 3) (Tindale et al., 1998; Reeve et al., 2016). A series of regional unconformities developed between the Valanginian and Hauterivian (i.e. the intra-Valanginian, top Valanginian, and intra-Hauterivian unconformities), which occur towards the base of the Winning Group, locally truncate underlying Triassic, Jurassic, and Early Cretaceous strata (Figs 3 and 4) (e.g., Tindale et al., 1998; Longley et al., 2002; Reeve et al., 2016).

Magmatic activity was only associated with the Late Jurassic-to-Early Cretaceous rift phase (Fig. 3) (Mihut and Müller, 1998; Symonds et al., 1998; Magee et al., 2013a; Magee et al., 2013b). At this time, two areally extensive (both >60,000 km^2) networks of interconnected sills (i.e. a sill-complex) were emplaced in the Exmouth Plateau and the Exmouth Sub-basin (Fig. 2A) (Symonds et al., 1998; Magee et al., 2013a; McClay et al., 2013; Rohrman, 2013). Sills are expressed on seismic data as very high-amplitude, saucer-shaped reflections that commonly occur in the Dingo Claystone (Figs 3 and 4) (Magee et al., 2013a; Magee et al., 2013b). Only one forced fold, which is underlain by a saucer-shaped sill and occurs in the Exmouth Sub-basin, has been previously identified in the area (Fig. 4) (Magee et al., 2013a).

DATASET AND METHODOLOGY

This study utilizes five, zero-phase, time-migrated, 2D seismic reflection surveys (Skorpion 2D MSS, Exmouth South, HE94, Chimaera 2D MSS, and Jawa MSS) that cover an area of *c.* 25,000 km^2 (Fig. 2B). The area of interest is located towards the western margin of the

Exmouth Sub-basin and covers *c*. 1600 km^2, within which line spacing ranges from 0.5–6 km (Fig. 2B). Data are displayed with either a normal or reverse polarity; i.e. a downward increase in acoustic impedance correlates to a positive, red or negative, blue reflection respectively. Borehole data from Blackdragon-1 and Falcone-1A were used to constrain lithology and age of regionally extensive strata; there is no well data in the immediate vicinity of the study area.

In addition to the mapping of sills, which are expressed as strata-discordant packages of very high-amplitude reflections, we interpret six key stratigraphic horizons (A-F). Two-way time structure maps and thickness (isochron) maps constrain the geometry and location of intrusion-induced forced folds. Horizons E and F likely correspond to the major intra-Valanginian and intra-Hauterivian unconformities, respectively (Fig. 4). The age and lithology of the strata below and between horizons A-E are difficult to constrain because no boreholes locally penetrate the interval of interest (Fig. 2B) and the horizons are laterally restricted so cannot be traced to nearby wells (e.g., Blackdragon-1 or Falcone-1A; Fig. 2B). However, we note that the seismic character and depth of the interval of interest is comparable to that of the area studied by Magee et al. (2013a), which is located *c*. 30 km to the east, near (<7 km) the Falcone-1A well in the Central Exmouth Sub-basin (Figs 2B and 4). We infer that the two isolated depocenters (i.e. the Northern and Central Sub-basins) contain similar stratigraphic sequences due to the very similar seismic facies they contain; we thus use borehole data from Falcone-1A to infer the composition and age of the succession encountered in the interval of interest (Figs 2B and 4). Based on this inference, we tentatively interpret the intruded host rock succession in the Northern Exmouth Sub-basin consists of Dingo Claystone (Upper Jurassic) and, possibly, Barrow Group (Early Cretaceous) strata (Fig. 4). The presence of a relatively thick Jurassic sequence in the western part of the Northern Exmouth Sub-basin is consistent with previous recognition of a southward thickening of Jurassic strata within the Exmouth Plateau towards the Cape Range Fracture Zone (Stagg et al., 2004). However, borehole data are required to test whether the Jurassic-to-Early Cretaceous succession extends into the Northern Exmouth Sub-basin and, if so, the relative thicknesses of the different formations.

The Dingo Claystone has an interval velocity of 2.20 km s^{-1} (±10%) (Magee et al., 2013a) and, based on a dominant seismic frequency of ~46 Hz (ranging from ~40–50 Hz) across the five seismic surveys, we suggest that the limit of separability of the host rock is ~12 m, but may vary slightly from ~10–15 m. Where magmatic bodies are imaged in the Skorpion 2D MSS, Exmouth South, and Jawa MSS seismic surveys, the dominant frequency of the data decreases to ~23 Hz (ranging from ~20–25 Hz). In these locations, by assuming an interval velocity of 5.55 km s^{-1} (±10%) for the igneous intrusions (Skogly, 1998; Magee et al., 2015), the measured dominant frequency suggest that the top and base intrusive contacts are only represented by discrete reflections when sill thickness is ~>60 m; this value may range from ~56–69 m if variability in the dominant frequencies and error in interval velocities is taken into account. Below this thickness, interference between top and base intrusive contact reflections will occur, producing a tuned reflection package, and the true sill thickness will be uncertain (Smallwood and Maresh, 2002; Thomson, 2005; Magee et al., 2015; Planke et al. 2015). Sills are characterized by high acoustic impedance values, i.e. high density and high seismic velocity, and they thus absorb a large amount of seismic energy. Because of this, underlying geological features, including deeper sills, may be poorly imaged beneath the uppermost, better-imaged sills. We therefore have greater confidence in mapping sills and forced folds developed at the top of intrusive networks; the sill-fold pairs studied here occur at the top of their related intrusive networks.

RESULTS

Host rock structure

Horizon A

The eastern limit of the lowermost horizon mapped, Horizon A, is marked by a major W-dipping normal fault (Figs 4 and 5); Horizon A cannot be identified in the footwall of this fault. It is difficult to map Horizon A further north or south due to a decrease in data quality. In the west, high-amplitude reflections, which we infer are the seismic expression of sills, commonly inhibit imaging of Horizon A and underlying reflections (Figs 6A and B). Overall, Horizon A dips gently north-westwards (Fig. 5). In the south, a ~3 km diameter, dome-shaped fold (i.e. Fold 1), with an amplitude of ~217 ms TWT (~239 m), is superimposed on Horizon A (Figs 5, 6C and D). Along the outer portions of Fold 1, Horizon A is cross-cut by a package of saucer-shaped, high-amplitude sill reflections (e.g., Fig. 6C). Horizon A is also locally uplifted in the center of the study area (i.e. Fold 2), where it is directly underlain by a package of high-amplitude reflections that are physically separate from those underlying Fold 1 (Figs 6A and E). Because we cannot map the full lateral extent of Horizon A, it is difficult to determine the geometry of Fold 2 at this stratigraphic level (Fig. 5). With the exception of the seismic reflections immediately underlying Horizon A, there is no evidence that deeper reflections are folded and/or uplifted (Figs 6A-D).

Horizon B

Horizon B is bound to the east by a W-dipping normal fault and the remainder of its mapped extent is constrained by a reduction in data quality, commonly associated with overlying, transgressive, high-amplitude sill-related reflections (Figs 5 and 6D). Overall, Horizon B dips gently to the NW (Fig. 5). Along Horizon B, there is a clear dome-shaped fold (i.e. Fold 1) that has a diameter of *c*. 4 km, an amplitude of ~267 ms TWT (~294 m), and is apparently bound by a sub-vertical, circumferential fault that seemingly overlies the lateral tips of a sill (Figs 5, 6C and D). Compared to the more circular Fold 1, Fold 2 is defined by a more ovate region of uplift (>15 km long and up to 13 km wide), is of lower amplitude (~159 ms TWT or ~175 m), and does not appear to be bound by a fault (Figs 5, 6A and B). Between horizons A and B, divergent reflections indicate that the stratigraphic package thickens by up to ~674 ms TWT (~741 m) towards the center of the study area (Figs 5 and 6A-D).

Horizon C

The eastern limit of Horizon C is partly defined by a W-dipping major fault, whereas to the south and south-east it is truncated by Horizon E (Fig. 5). Horizon C dips gently to the NW (Fig. 5). Folds 1 and 2 are expressed along Horizon C; Fold 1 has a diameter of ~4.5 km and an amplitude of ~249 ms TWT (~274 m), whereas Fold 2 is >17 km long, ~13 km wide, and has an amplitude of ~148 ms TWT (~163 m) (Figs 5 and 6). Parts of Fold 1 expressed along Horizon A appear to be bound by the same circumferential fault that displace Horizon B (Figs 5, 6C and D). For example, along the southern limit of Fold 1, it may be considered that the high-amplitude Horizon C reflection is offset across a fault (Fig. 6C and Appendix A). However, directly above the suggested hanging wall termination of Horizon C, there are a series of southward-dipping that appear continuous across the fault and downlap onto Horizon C (Fig. 6C and Appendix A); it may be argued that these dipping reflectors are indicative of folding, implying that the top of the folded strata, including Horizon C, is not faulted. Based on comparison to Horizon B, we favor that Horizon C is faulted and that the apparent dipping reflectors are either: (1) a geophysical artefact (e.g., poor migration or sideswipe); or (2) sediment shed off the forced fold during doming. Reflections between horizons B and C are broadly parallel and there is little change in thickness of the stratal unit across the study area (Figs 5 and 6A-D). To the south and south-east of Fold 1, Horizon C has a higher amplitude compared to elsewhere in the study area and is underlain by a zone of high-amplitude, chaotic reflections.

Horizon D

Horizon D is laterally restricted and dips to the N (Fig. 5). The stratigraphic package bound by horizons C and D contains a series of parallel reflections that onlap onto and intersect Horizon C at a high angle, except at its southern limit where the strata is truncated by Horizon E (Figs 5 and 6B-D). A key observation is that this stratigraphic package onlaps onto and subtly thickens towards folds 1 and 2 expressed along Horizon C (Figs 5, 6C and D).

Horizon E

Horizon E, the intra-Valanginian unconformity, dips gently to the NW and truncates underlying reflections (Figs 5 and 6A-B). To the NW, it is difficult to map the intra-Valanginian unconformity due to a decrease in data quality and coverage (Fig. 5). To the SW, Horizon E is itself truncated by the intra-Hauterivian unconformity (i.e. Horizon F; Figs 5, 6A, C, and D). Strata bounded by horizons D and E apparently thickens south-westwards towards Fold 1 (Fig. 5). Reflections within the horizon D-E sedimentary package are not folded but rather onlap onto and thin across Fold 1 (Figs 6C, D, and 7); immediately adjacent to Fold 1, these reflections dip moderately away from the fold (Fig. 6C).

Horizon F

Horizon F corresponds to the intra-Hauterivian unconformity (Fig. 4). In the south-west of the study area, Horizon F dips gently northwards into an elliptical depression (Figs 5 and 6A). The stratigraphic package between horizons E and F thickens northwards (Fig. 5).

Faults

In addition to the major W-dipping normal fault that defines the eastern limit of horizons A-C, numerous normal faults are observed across the study area, both within and beyond the folded strata (Figs 6A-D). These normal faults display low displacements (<30 ms TWT) and are typically located between horizons A-C, although some extend below Horizon A and/or up to Horizon E (Figs 6A-D). The majority of these faults appear to have throw maxima near the fault center, but those within Fold 1 display maximum throw at their upper tips, which typically coincide with Horizon C (Figs 6C and D). A sub-vertical, circumferential fault appears to partly define the limits of Fold 1, displacing horizons B and C (Figs 5 and 6C). Only one W-dipping normal fault offsets Horizon F; this has a displacement of ~67 ms TWT (~74 m) and nearly reaches the seabed (Fig. 6D).

Sills

We identify a series of discontinuous, high-amplitude seismic reflections, clustered and vertically stacked within an area of ~210 km^2 and spanning a depth range of 2.7–3.9 s TWT. We interpret these reflections as being the seismic expression of sills (Fig. 6) (e.g., Smallwood and Maresh, 2002; Magee et al., 2015). The majority of sills appear to be expressed as discrete tuned reflection packages (i.e. their top and base contacts cannot be distinguished), indicating that their thickness is below the calculated limit of separability of *c.* 60 m. Sill reflections are typically saucer-shaped and can be sub-divided into a strata-concordant central portion, which typically coincides with Horizon A, fully or partly surrounded by an inwardly inclined sheet that transgresses stratigraphy (Figs 6A-D). Some intrusion-related reflections have a planar, inclined sheet morphology (e.g., Fig 6B). It is possible that some high-amplitude reflections beneath the shallowest sills may represent intrusion-related multiples (Figs 6A-D).

The mapped outlines of folds 1 and 2 are typically directly underlain by the lateral termination of one or several sills (Fig. 6). For example, the boundary of Fold 1 coincides with the lateral termination of a zone bound at its top and base by well-defined, very high-amplitude reflections that have a saucer-shaped morphology, a diameter of ~4.2 km, and a transgressive height of up to ~ 247 ms TWT (~271 m) (Figs 6C, D, and F). This zone is up to ~316 ms TWT (~877 m) thick, thinning towards its lateral terminations, and contains a series of very high-amplitude, saucer-shaped reflections (Figs 6C and D). Sills clustered beneath Fold 2 are ~4–15 km long and appear to be interconnected (Figs 6A-E).

INTERPRETATION AND DISCUSSION

We interpret that folds 1 and 2 represent intrusion-induced forced folds generated in response to roof uplift above intruding and inflating sills because: (1) the fold outlines correspond closely to the lateral terminations of underlying sills (Fig. 6E) (Pollard and Johnson, 1973; Hansen and Cartwright, 2006; Galland and Scheibert, 2013; Magee et al., 2013c; Magee et al., 2014); and (2) no evidence of folding beneath the sills is observed, suggesting that deformation was not related to regional horizontal shortening (e.g., Figs 6A-D). Here, we discuss when folding occurred, the mechanics of deformation, and the response of onlapping strata to changes in fold geometry. We also consider the importance of sill-related forced folds for petroleum systems development.

Onset of forced folding and timing of sill emplacement

Westward thickening of the stratigraphic package bound by horizons A and B occurs across and beyond the limits of folds 1 and 2, indicating that this thickness trend is a regional pattern unrelated to folding (Figs 5 and 6A-D). In contrast, there is little variation in the thickness of horizon B-C across folds 1 and 2 (Figs 5 and 6A-D). The lack of local thickening patterns associated with folds 1 and 2 implies that the package bound by horizons A and C was deposited prior to sill-induced deformation. Younger strata (i.e. post-Horizon C), however, onlap onto the top of the forced folds (i.e. Horizon C), indicating that folding had occurred and a bathymetric expression attained prior to their deposition (Figs 5-6) (e.g., Trude et al., 2003; Hansen and Cartwright, 2006). These seismic-stratigraphic observations suggest that initial fold formation, and thus sill emplacement, occurred when Horizon C represented the paleoseabed (Fig. 8) (Trude et al., 2003; Magee et al., 2014). We also interpret that the southern, high-amplitude portion of Horizon C, where it is underlain by a thin zone of high-amplitude chaotic reflections, as a lava flow (e.g., Fig. 6C) (Planke et al., 2000). Constraining the absolute age of Horizon C is difficult, however, because it cannot be directly mapped across to areas penetrated by boreholes (Figs 4 and 5). Nevertheless, based on comparison between the seismic character and apparent stratigraphic level of the forced folds studied here and one observed further to the east in the Exmouth Sub-basin near the Falcone-1A well (Fig. 4), we tentatively suggest that sill emplacement and folding possibly occurred in the Kimmeridgian-to-Tithonian (Magee et al., 2013a). Our inferred timing of magmatic activity is supported by two dredged samples of basaltic andesite and rhyolite samples, obtained from the Exmouth Sub-basin ~80 km SW of the study area, which have approximate ages of 150 Ma (Dadd et al., 2015).

Mechanics of forced folding

Intrusion-induced forced folds are traditionally considered to form through elastic bending of the overburden in response to sill injection and inflation (e.g., Pollard and Johnson, 1973; Goulty and Schofield, 2008). Models invoking elastic bending predict that the volume of host rock deformation and emplaced magma should be equal, implying that the amplitude of a forced fold mirrors underlying sill thickness (Hansen and Cartwright, 2006). However, recent work has demonstrated that other mechanisms (e.g., compaction, fluidization, and faulting), which inelastically deform the host rock and may produce a mismatch between fold amplitude and sill thickness, can accommodate intrusion and fold development (e.g., Schofield et al., 2012; Jackson et al., 2013; Magee et al., 2013a; Wilson et al., 2016). Because inelastic deformation can degrade or enhance host rock permeability, it is critical to constrain the mechanics of sill emplacement and fold growth in order to evaluate intrusion-induced forced folds as viable hydrocarbon traps.

Fold 1 has an amplitude of *c*. 274 m and appears to be underlain by a saucer-shaped sill with a calculated thickness of *c*. 877 m (Fig. 6); fold amplitude is thus only ~69% of the estimated sill thickness. Magee et al. (2013a) reported that the sill-fold pair imaged further east in the Exmouth-Sub-basin also displayed a discrepancy (*c*. 40%) between fold amplitude (*c*. 150 m) and sill thickness (*c*. 283 m), which they attributed to porosity reduction induced by pore fluid expulsion from the Dingo Claystone host rock (Fig. 4). Whilst the difference between Fold 1 amplitude and sill thickness may be partly attributable to a similar fluidization process (see Magee et al., 2013a), we consider it unlikely that a mismatch of *c*. 603 m (i.e. 69%) can be solely related to porosity reduction. Furthermore, the occurrence of internal reflections between the mapped upper and lower boundaries of the mapped zone requires the presence of several interfaces demarcating significant acoustic impedance contrasts (Fig. 6C). We suggest that the imaging of these internal reflections, which could correspond to rock-rock boundaries, tuned reflection packages, or ringing, indicates the presence of interfaces between multiple saucer-shaped sills and intervening slivers of host rock. This hypothesis is supported by borehole and seismic data from the Faroe-Shetland Basin, NE Atlantic, which show that stacked sills separated by sedimentary strata produces a zone of high reflectivity (Archer et al., 2005; Schofield et al., 2015). Importantly, the suggested occurrence of sedimentary rock slivers within the mapped boundary of the sill implies that the cumulative thickness of intruded magma is <877 m. The interval velocity of a package of sills and sedimentary rocks will also be reduced (i.e. <5.55 km s^{-1}), further implying that a calculated thickness of 877 m overestimates the actual cumulative thickness of intrusive material. Due to these difficulties in elucidating the actual thickness of sills relative to fold amplitude, it is thus difficult to quantify the role of inelastic deformation without borehole data.

Faulting, in addition to the potential reduction in host rock porosity, has influenced the structure of Fold 1 (Figs 6A-D). For example, the flank of Fold 1 is partly defined by a steep, sub-vertical fault that, in addition to folding, accommodated uplift of strata above the sill overburden (Figs 5, 6C and 8). Furthermore, we interpret that the normal faults within

Fold 1 are related to outer-arc extension because: (1) the upper fault tips coincide with Horizon C, the top of Fold 1 (Figs 6C-D) (Jackson et al., 2013; Magee et al., 2013a); and (2) fault throw is greatest at Horizon C, decreasing with depth (Figs 6A-D), implying that the faults nucleated at the outermost part of the fold crest before propagating downwards (Mathieu et al., 2008; Galland, 2012; Galland and Scheibert, 2013). Outer-arc extension faults form during folding in response to extensional strains that are greatest at the crest of the fold (Cosgrove and Hillier, 1999; Galland and Scheibert, 2013). In the study area, these outer-arc extension faults are thus synchronous to fold development and sill emplacement (i.e. Kimmeridgian).

A network of stacked, overlapping sills (i.e. a sill-complex) underlie Fold 2 suggesting that this structure can be classified as a 'compound fold' that formed through the coalescence of smaller, individual forced folds (Magee et al., 2014). Although the development of compound folds produce four-way dip closures that cover a greater areal extent than individual forced folds, the processes dictating internal deformation within them remain poorly constrained (Magee et al., 2014). The normal faults within Fold 2 are not constrained to the folded strata (i.e. many extend above Horizon C) and, similar to those observe in strata beyond the folds, are likely tectonic faults that nucleated during Early Cretaceous rifting (Magee et al., 2016a).

Stratigraphic record of forced fold growth

Forced folds are expressed at the surface during their growth (e.g., Trude et al., 2003; Holford et al., 2012), thus the seismic-stratigraphic architecture of onlapping strata may provide insights into their growth (Magee et al., 2014). For example, it is clear that the stratal package C-D, which onlaps onto Fold 1, maintains a relatively uniform thickness across the study area and that Horizon D does not deviate from its regional, gentle northwards dip (Figs 5 and 6B-D); these observations imply that Fold 1 grew rapidly prior to deposition of horizons C-D (Fig. 8). However, reflections overlying Horizon D, which onlap onto Horizon C, appear draped across Fold 1 (Fig. 6C). We therefore suggest that these sediments were deposited during a renewed phase of Fold 1 growth, following a period of quiescence marked by the deposition of strata bound by horizons C-D, likely associated with the injection of new sills (Fig. 8). Importantly, our interpretation of protracted fold growth implies that sill emplacement occurred incrementally and not instantaneously (Magee et al., 2014). Constraining the age of the lowermost reflections that onlap onto intrusion-induced forced folds can therefore only be used to define the onset of sill emplacement and not its duration (cf. Trude et al., 2003; Hansen and Cartwright, 2006; Jackson et al., 2013; Magee et al., 2013a)

Impact of forced folding on petroleum systems

Folds 1 and 2 can be described as four-way dip closures and may therefore represent hydrocarbon exploration targets (Fig. 5). A successful evaluation of a four-way dip closure as a hydrocarbon trap relies on constraining: (1) when the four-way dip closure formed relative to hydrocarbon generation and migration; (2) whether fold growth impacted or generate a local fault and fracture networks; and (3) whether it influenced syn-kinematic sedimentation patterns and the distribution of reservoir rocks. Given that hydrocarbon generation and migration in the Exmouth Sub-basin occurred in the Early Cretaceous (Tindale et al., 1998), it is plausible that the Kimmeridgian aged, intrusion-induced forced folds could have trapped migrating hydrocarbons if they contain suitable reservoir horizons and if a seal was in-place (e.g., Fig. 9). Furthermore, the occurrence of at-surface relief may have influenced sediment routing systems and/or generated stratigraphic traps related to stratal onlap (Fig. 9) (e.g., Smallwood and Maresh, 2002; Holford et al., 2012; Magee et al., 2014). Within Fold 1, a series of normal faults have been identified that formed during fold growth in response to outer-arc extension (Figs 6C and D). Such faults may potentially compartmentalize any reservoirs within Fold 1 and, depending on their damage zone properties, could also provide local seals within a forced fold or facilitate hydrocarbon leakage (Fig. 9) (Reeckmann and Mebberson, 1984).

CONCLUSION

Sills emplaced at shallow-levels in sedimentary basins are commonly accommodated by overburden uplift and the formation of four-way dip closures, termed intrusion-induced forced folds. These four-way dip closures have received little interest from the petroleum industry, due to the risks associated with igneous-related prospects, despite the occurrence of several producing fields worldwide that exploit intrusion-induced forced folds. Here, we examine two forced folds above a series of sills imaged in 2D seismic reflection data from the Exmouth Sub-basin, offshore NW Australia. Seismic-stratigraphic onlap relationships indicate that fold development, and thereby sill emplacement, likely occurred in the Kimmeridgian prior to Early Cretaceous hydrocarbon generation and migration. In addition to forced folding, it is likely that part of the intruded magma volume was accommodated by inelastic deformation, including porosity reduction induced by host rock fluidization and outer-arc faulting, of the folded strata. Variations in the vertical structure of reflections that onlap onto the forced folds, at different stratigraphic levels, implies that fold formation was not instantaneous but grew over a period of time in response to incremental magma intrusion. The age of the lowermost horizons to onlap intrusion-induced forced folds can therefore only be used to determine the onset of sill emplacement, not its duration. We show that intrusion-induced forced folds can form important hydrocarbon traps but that it is critical to evaluate the growth mechanics of such structures in order to de-risk exploration targets.

ACKNOWLEDGEMENTS

Geoscience Australia are thanked for providing the seismic and borehole data and Schlumberger for the provision of interpretation software. CM is supported by a Junior Research Fellowship at Imperial College London. We are grateful to Max Rohrman and John Millet for their constructive reviews and Simon Holford and Kurt Marfurt for editorial handling.

APPENDIX A

Uninterpreted seismic sections used in Figure 6A-D

REFERENCES

Agirrezabala, L. M., 2015, Syndepositional forced folding and related fluid plumbing above a magmatic laccolith: Insights from outcrop (Lower Cretaceous, Basque-Cantabrian Basin, western Pyrenees): Geological Society of America Bulletin, B31192. 1.

Archer, S. G., S. C. Bergman, J. Iliffe, C. M. Murphy, and M. Thornton, 2005, Palaeogene igneous rocks reveal new insights into the geodynamic evolution and petroleum potential of the Rockall Trough, NE Atlantic Margin: Basin Research, **17**, 171-201.

Cosgrove, J. W., and R. D. Hillier, 1999, Forced-fold development within Tertiary sediments of the Alba Field, UKCS: evidence of differential compaction and post-depositional sandstone remobilization: Geological Society, London, Special Publications, **169**, 61-71.

Dadd, K. A., L. Kellerson, I. Borissova, and G. Nelson, 2015, Multiple sources for volcanic rocks dredged from the Western Australian rifted margin: Marine Geology, **368**, 42-57.

Exon, N., B. Haq, and U. Von Rad, 1992, Exmouth Plateau revisited: scientific drilling and geological framework: Proceedings of the Ocean Drilling Program, Scientific Results, p. 3-20.

Galland, O., 2012, Experimental modelling of ground deformation associated with shallow magma intrusions: Earth and Planetary Science Letters, **317**, 145-156.

Galland, O., and J. Scheibert, 2013, Analytical model of surface uplift above axisymmetric flat-lying magma intrusions: Implications for sill emplacement and geodesy: Journal of Volcanology and Geothermal Research, **253**, 114-130.

Gilbert, G. K., 1877, Report on the Geology of the Henry Mountains, US Government Printing Office.

Goulty, N. R., and N. Schofield, 2008, Implications of simple flexure theory for the formation of saucer-shaped sills: Journal of Structural Geology, **30**, 812-817.

Hansen, D. M., and J. Cartwright, 2006, The three-dimensional geometry and growth of forced folds above saucer-shaped igneous sills: Journal of Structural Geology, **28**, 1520-1535.

Hansen, D. M., J. Redfern, F. Federici, D. di Biase, and G. Bertozzi, 2008, Miocene igneous activity in the Northern Subbasin, offshore Senegal, NW Africa: Marine and Petroleum Geology, **25**, 1-15.

Hocking, R., 1992, Jurassic deposition in the southern and central North West Shelf: Western Australia: Geological Survey Western Australia Record, **199217**.

Hocking, R. M., H. T. Moors, and W. E. Van de Graaff, 1987, Geology of the carnarvon basin, Western Australia, v. 133, State Print. Division.

Holford, S. P., N. Schofield, J. D. MacDonald, I. R. Duddy, and P. F. Green, 2012, Seismic analysis of igneous systems in sedimentary basins and their impacts on hydrocarbon prospectivity: examples from the southern Australian margin: APPEA Journal, **52**, 23.

Jackson, C. A.-L., N. Schofield, and B. Golenkov, 2013, Geometry and controls on the development of igneous sill–related forced folds: A 2-D seismic reflection case study from offshore southern Australia: Geological Society of America Bulletin, **125**, 1874-1890.

Johnson, A. M., and D. D. Pollard, 1973, Mechanics of growth of some laccolithic intrusions in the Henry mountains, Utah, I: field observations, Gilbert's model, physical properties and flow of the magma: Tectonophysics, **18**, 261-309.

Longley, I., C. Buessenschuett, L. Clydsdale, C. Cubitt, R. Davis, M. Johnson, N. Marshall, A. Murray, R. Somerville, and T. Spry, 2002, The North West Shelf of Australia–a Woodside perspective: The sedimentary basins of Western Australia, **3**, 27-88.

Magee, C., F. Briggs, and C. A.-L. Jackson, 2013a, Lithological controls on igneous intrusion-induced ground deformation: Journal of the Geological Society, **170**, 853-856.

Magee, C., C. A.-L. Jackson, and N. Schofield, 2013b, The influence of normal fault geometry on igneous sill emplacement and morphology: Geology, **41**, 407-410.

Magee, C., E. Hunt-Stewart, and C. A. L. Jackson, 2013c, Volcano growth mechanisms and the role of sub-volcanic intrusions: Insights from 2D seismic reflection data: Earth and Planetary Science Letters, **373**, 41-53.

Magee, C., C. L. Jackson, and N. Schofield, 2014, Diachronous sub-volcanic intrusion along deep-water margins: insights from the Irish Rockall Basin: Basin Research, **26**, 85-105.

Magee, C., S. M. Maharaj, T. Wrona, and C. A.-L. Jackson, 2015, Controls on the expression of igneous intrusions in seismic reflection data: Geosphere, GES01150. 1.

Magee, C., O. B. Duffy, K. Purnell, R. E. Bell, C. A. L. Jackson, and M. T. Reeve, 2016a, Fault-controlled fluid flow inferred from hydrothermal vents imaged in 3D seismic reflection data, offshore NW Australia: Basin Research, **28**, 19.

Magee, C., J. D. Muirhead, A. Karvelas, S. P. Holford, C. A. Jackson, I. D. Bastow, N. Schofield, C. T. Stevenson, C. McLean, and W. McCarthy, 2016b, Lateral magma flow in mafic sill complexes: Geosphere, GES01256. 1.

Mathieu, L., B. van Wyk de Vries, E. P. Holohan, and V. R. Troll, 2008, Dykes, cups, saucers and sills: Analogue experiments on magma intrusion into brittle rocks: Earth and Planetary Science Letters, **271**, 1-13.

McClay, K., N. Scarselli, and S. Jitmahantakul, 2013, Igneous intrusions in the Carnarvon Basin, NW Shelf, Australia, *in* M. Keep, and S. J. Moss, eds., The Sedimentary Basins of Western Australia IV, Proceedings of the Petroleum Exploration Society of Australia Symposium.

Mihut, D., and R. D. Müller, 1998, Volcanic margin formation and Mesozoic rift propagators in the Cuvier Abyssal Plain off Western Australia: Journal of Geophysical Research, **103**, 27135-27,149.

Müller, R., D. Mihut, C. Heine, C. O'Neill, and I. Russell, 2002, Tectonic and volcanic history of the Carnarvon Terrace: Constraints from seismic interpretation and geodynamic modelling: The Sedimentary Basins of Western Australia, **3**, 719-740.

Planke, S., P. A. Symonds, E. Alvestad, and J. Skogseid, 2000, Seismic volcanostratigraphy of large-volume basaltic extrusive complexes on rifted margins: Journal of Geophysical Research: Solid Earth, **105**, 19335-19351.

Planke, S., H. Svensen, R. Myklebust, S. Bannister, B. Manton, and L. Lorenz, 2015, Geophysics and Remote Sensing, Springer Berlin Heidelberg, 1-16.

Pollard, D. D., and A. M. Johnson, 1973, Mechanics of growth of some laccolithic intrusions in the Henry Mountains, Utah, II: bending and failure of overburden layers and sill formation: Tectonophysics, **18**, 311-354.

Polteau, S., A. Mazzini, O. Galland, S. Planke, and A. Malthe-Sørenssen, 2008, Saucer-shaped intrusions: occurrences, emplacement and implications: Earth and Planetary Science Letters, **266**, 195-204.

Reeckmann, S. A., and A. J. Mebberson, 1984, Igneous intrusions in the North-West Canning Basin and their impact on oil exploration, *in* P. G. Purcell, ed., The Canning Basin, WA, Proceedings of the Geological Society of Australia/Petroleum Exploration Society of Australia Canning Basin Symposium, 389-399.

Reeve, M. T., C. A. L. Jackson, R. E. Bell, C. Magee, and I. D. Bastow, 2016, The stratigraphic record of prebreakup geodynamics: Evidence from the Barrow Delta, offshore Northwest Australia: Tectonics.

Rodriguez Monreal, F., H. Villar, R. Baudino, D. Delpino, and S. Zencich, 2009, Modeling an atypical petroleum system: a case study of hydrocarbon generation, migration and accumulation related to igneous intrusions in the Neuquen Basin, Argentina: Marine and Petroleum Geology, **26**, 590-605.

Rohrman, M., 2013, Intrusive large igneous provinces below sedimentary basins: An example from the Exmouth Plateau (NW Australia): Journal of Geophysical Research: Solid Earth, **118**, 4477-4487.

Ross, M. I., and P. R. Vail, 1994, Sequence stratigraphy of the lower Neocomian Barrow Delta, Exmouth Plateau, northwestern Australia: The Sedimentary Basins of Western Australia: Proceedings of the Petroleum Exploration Society of Australia Symposium, Perth, p. 435-447.

Schofield, N. J., D. J. Brown, C. Magee, and C. T. Stevenson, 2012, Sill morphology and comparison of brittle and non-brittle emplacement mechanisms: Journal of the Geological Society, **169**, 127-141.

Schofield, N., S. Holford, J. Millett, D. Brown, D. Jolley, S. Passey, D. Muirhead, C. Grove, C. Magee, J. Murray, M. Hole, C. Jackson, and C. Stevenson, 2015, Regional Magma Plumbing and emplacement mechanisms of the Faroe-Shetland Sill Complex: Implications for magma transport and petroleum systems within sedimentary basins: Basin Research, 1-23.

Schutter, S. R., 2003, Hydrocarbon occurrence and exploration in and around igneous rocks: Geological Society, London, Special Publications, **214**, 7-33.

Skogly, O., 1998, Seismic characterization and emplacement of intrusives in the Vøring Basin: M.Sc. Thesis thesis, University of Oslo.

Smallwood, J. R., and J. Maresh, 2002, The properties, morphology and distribution of igneous sills: modelling, borehole data and 3D seismic from the Faroe-Shetland area, *in* D. W. Jolley, and B. R. Bell, eds., The North Atlantic Igneous Province: Stratigraphy, tectonic, Volcanic and Magmatic Processes, Geological Society, London, Special Publications 197, 271-306.

Stagg, H., and J. Colwell, 1994, The structural foundations of the Northern Carnarvon Basin: The sedimentary basins of Western Australia: Proceedings of Petroleum Exploration Society of Australia Symposium, Perth, p. 349-365.

Stagg, H., M. Alcock, G. Bernardel, A. Moore, P. Symonds, and N. Exon, 2004, Geological framework of the outer Exmouth Plateau and adjacent ocean basins, Geoscience Australia.

Stearns, D. W., 1978, Faulting and forced folding in the Rocky Mountains foreland: Geological Society of America Memoirs, **151**, 1-38.

Symonds, P. A., S. Planke, O. Frey, and J. Skogseid, 1998, Volcanic evolution of the Western Australian Continental Margin and its implications for basin development: The Sedimentary Basins of Western Australia 2: Proc. of Petroleum Society Australia Symposium, Perth, WA.

Thomson, K., 2005, Volcanic features of the North Rockall Trough: application of visualisation techniques on 3D seismic reflection data: Bulletin of Volcanology, **67**, 116-128.

Tindale, K., N. Newell, J. Keall, and N. Smith, 1998, Structural evolution and charge history of the Exmouth Sub-basin, northern Carnarvon Basin, Western Australia: The Sedimentary Basins of Western Australia 2: Proc. of Petroleum Society Australia Symposium, Perth, WA, p. 473-490.

Trude, J., J. Cartwright, R. J. Davies, and J. R. Smallwood, 2003, New technique for dating igneous sills: Geology, **31**, 4.

Wilson, P. I., K. J. McCaffrey, R. W. Wilson, I. Jarvis, and R. E. Holdsworth, 2016, Deformation structures associated with the Trachyte Mesa intrusion, Henry Mountains, Utah: Implications for sill and laccolith emplacement mechanisms: Journal of Structural Geology, **87**, 30-46.

LIST OF FIGURES

Figure 1: (A) Schematic diagram highlighting how roof uplift may accommodate an intruding sill and produce a forced fold, which may be expressed at the paleosurface and onlapped by younger strata (modified from Magee et al., 2014). (B) Map of showing the distribution of forced folds recorded above sills and/or laccoliths, some of which host hydrocarbon fields or shows (adapted from Magee et al., 2016b). The example forced folds documented are located in (inset sketches of forced folds redrawn from the respective reference for each area): (1) Irish Rockall Basin, offshore NW Ireland and specifically targeted by well 5/22-1 (Magee et al., 2014); (2) Faroe-Shetland Basin, NE Atlantic (Schofield et al., 2015); Møre Basin, offshore Norway and specifically above the Tulipan Sill (Polteau et al., 2008); (4) Pyrenees (Agirrezabala, 2015); (5) Northern Sub-basin, offshore Senegal (Hansen et al., 2008); (6) Danakil Depression, Ethiopia; (7) Wichian Basin, Thailand (Schutter, 2003); (8) Exmouth Sub-basin, offshore NW Australia (Magee et al., 2013a); (9) Canning Basin, offshore NW Australia (Reeckmann and Mebberson, 1984); (10) Bight Basin, offshore S Australia (Jackson et al., 2013); (11) Henry Mountains, Utah, USA (Gilbert, 1877; Pollard and Johnson, 1973); (12) Neuquen Basin, Argentina (Rodriguez Monreal et al., 2009). Style of the passive margins are also shown.

Figure 2: (A) Overview of the NW Australian margin highlighting the extent of Late Jurassic-to-Early Cretaceous sill-complexes and volcanism. COTZ corresponds to the Continent-Ocean Transition Zone and CRFZ is the Cape Range Fracture Zone. (B) Tectonic elements of the study area and a zoomed in viewing showing the distribution of seismic lines (black lines) used here. AA = Alpha Arch; MH = Macedon High; B = Bundegi Terrace; CR = Cape Range Peninsula; PS = Peedamullah Shelf; YR = Yanrey Ridge; MS = Merlinleigh Sub-basin. The Northern and Central elements of the Exmouth Sub-basin are highlighted. Tectonic element configuration taken from Reeve et al. (2016) and references therein.

Figure 3: Stratigraphic column for the study area (based on Symonds et al., 1998; Tindale et al., 1998; Longley et al., 2002; Magee et al., 2013a; Magee et al., 2016a).

Figure 4: Uninterpreted and interpreted composite seismic line depicting the regional geology. Letters C, E, and F correspond to locally mapped stratigraphic horizons. See Figure 3 for key. TWT = Two-way Time.

Figure 5: Two-way time structure maps for horizons A-F and thickness maps for the sedimentary packages bound by horizons A-B, B-C, C-D, D-E, and E-F. Contours spaced every 50 ms TWT. See Figure 2B for location. Thick. = Thickness.

Figure 6: (A-D) Interpreted seismic lines detailing the structure of the sills and associated folds 1 and 2. Fault displacement arrows omitted from tectonic normal faults for clarity. Colors of sills mapped across multiple seismic lines correspond to thick lines and are color-coded to Figure 2E. Thin red lines are sills that can only be confidently mapped along one seismic line. See Figure 6E for locations. Uninterpreted seismic lines are provided within Appendix A. (E) Location of mapped sills relative to the fold outlines mapped along Horizon C (see Fig. 5). (F) 3D view of Horizon C showing folds 1 and 2 and of the mapped sills. See Figure 6E for viewing direction.

Figure 7: Thickness map of the sedimentary package between horizons C and E. See Figure 2B for location.

Figure 8: Development of Fold 1, initially via doming and faulting. Emplacement of later, smaller sills can localize deformation within the forced fold, preferentially causing the folding of specific onlapping packages.

Figure 9: Schematic diagram showing how intrusion-induced forced folds may impact petroleum systems. See text for details.

Figure A-1: Uninterpreted detailing the structure of the sills and associated folds 1 and 2. See Figure 6A-D for interpreted sections and Figure 6E for location.

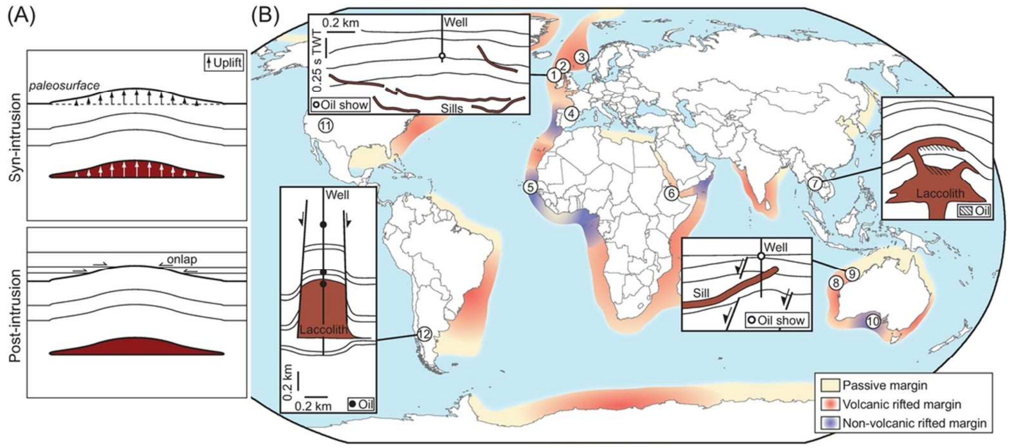

Figure 1: (A) Schematic diagram highlighting how roof uplift may accommodate an intruding sill and produce a forced fold, which may be expressed at the paleosurface and onlapped by younger strata (modified from Magee et al., 2014). (B) Map of showing the distribution of forced folds recorded above sills and/or laccoliths, some of which host hydrocarbon fields or shows (adapted from Magee et al., 2016b). The example forced folds documented are located in (inset sketches of forced folds redrawn from the respective reference for each area): (1) Irish Rockall Basin, offshore NW Ireland and specifically targeted by well 5/22-1 (Magee et al., 2014); (2) Faroe-Shetland Basin, NE Atlantic (Schofield et al., 2015); Møre Basin, offshore Norway and specifically above the Tulipan Sill (Polteau et al., 2008); (4) Pyrenees (Agirrezabala, 2015); (5) Northern Sub-basin, offshore Senegal (Hansen et al., 2008); (6) Danakil Depression, Ethiopia; (7) Wichian Basin, Thailand (Schutter, 2003); (8) Exmouth Sub-basin, offshore NW Australia (Magee et al., 2013a); (9) Canning Basin, offshore NW Australia (Reeckmann and Mebberson, 1984); (10) Bight Basin, offshore S Australia (Jackson et al., 2013); (11) Henry Mountains, Utah, USA (Gilbert, 1877; Pollard and Johnson, 1973); (12) Neuquen Basin, Argentina (Rodriguez Monreal et al., 2009). Style of the passive margins are also shown.

Fig. 1

101x44mm (300 x 300 DPI)

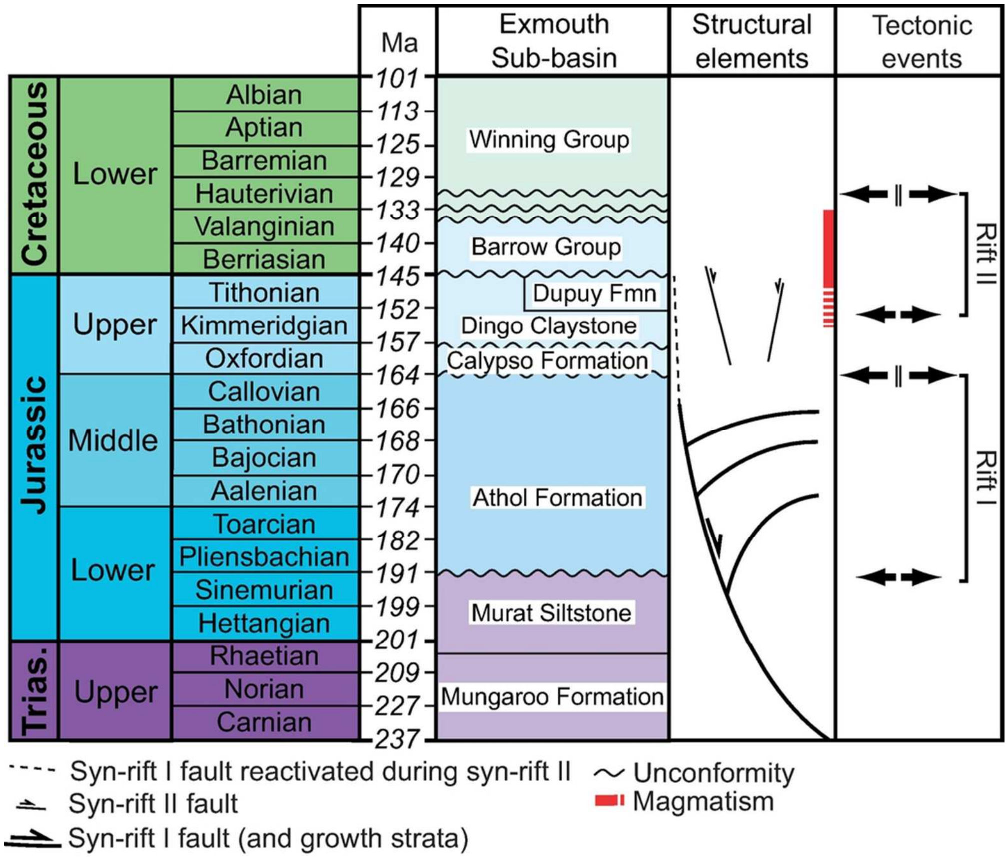

Figure 3: Stratigraphic column for the study area (based on Symonds et al., 1998; Tindale et al., 1998; Longley et al., 2002; Magee et al., 2013a; Magee et al., 2016a).
Fig. 3
87x74mm (300 x 300 DPI)

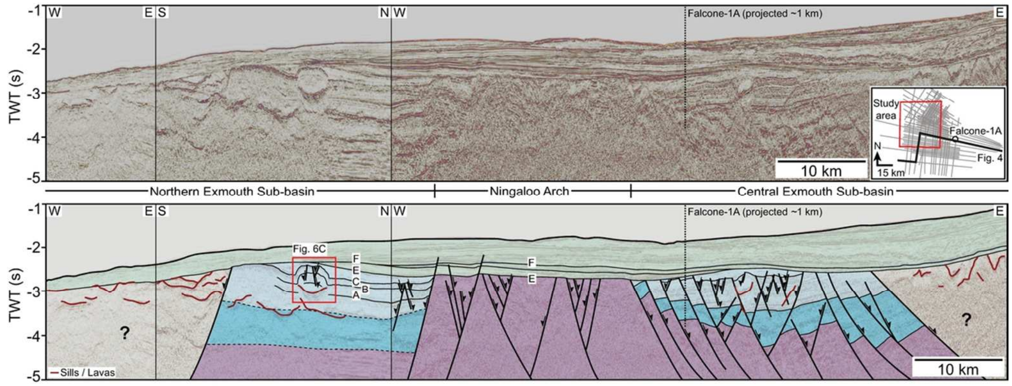

Figure 4: Uninterpreted and interpreted composite seismic line depicting the regional geology. Letters C, E, and F correspond to locally mapped stratigraphic horizons. See Figure 3 for key. TWT = Two-way Time.
Fig. 4
106x40mm (300 x 300 DPI)

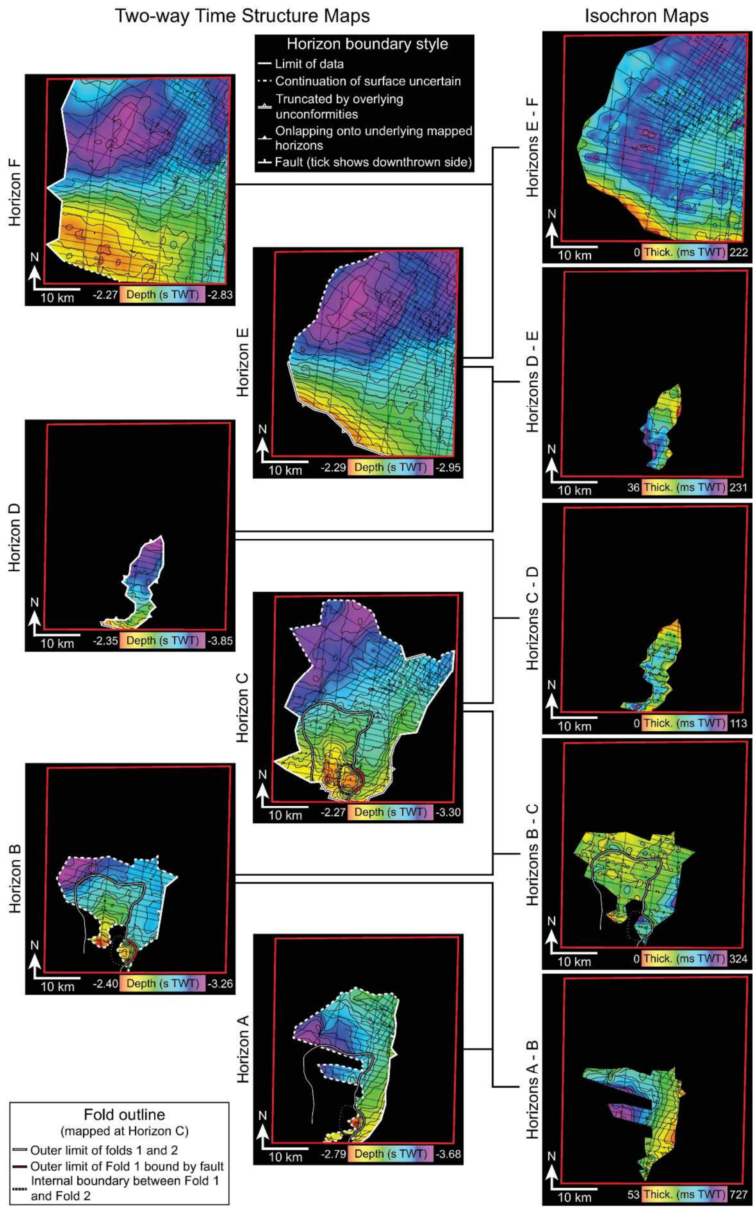

Figure 5: Two-way time structure maps for horizons A-F and thickness maps for the sedimentary packages bound by horizons A-B, B-C, C-D, D-E, and E-F. Contours spaced every 50 ms TWT. See Figure 2B for location. Thick. = Thickness.

Fig. 5

267x429mm (300 x 300 DPI)

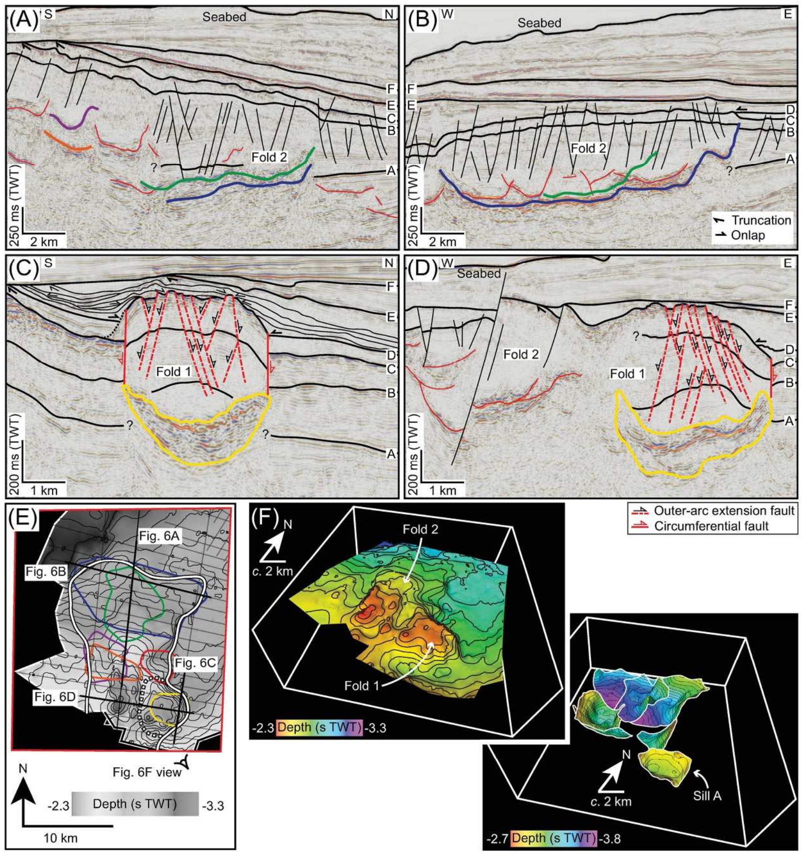

Figure 6: (A-D) Interpreted seismic lines detailing the structure of the sills and associated folds 1 and 2. Fault displacement arrows omitted from tectonic normal faults for clarity. Colors of sills mapped across multiple seismic lines correspond to thick lines and are color-coded to Figure 2E. Thin red lines are sills that can only be confidently mapped along one seismic line. See Figure 6E for locations. Uninterpreted seismic lines are provided within Appendix A. (E) Location of mapped sills relative to the fold outlines mapped along Horizon C (see Fig. 5). (F) 3D view of Horizon C showing folds 1 and 2 and of the mapped sills. See Figure 6E for viewing direction.

Fig. 6

195x174mm (300 x 300 DPI)

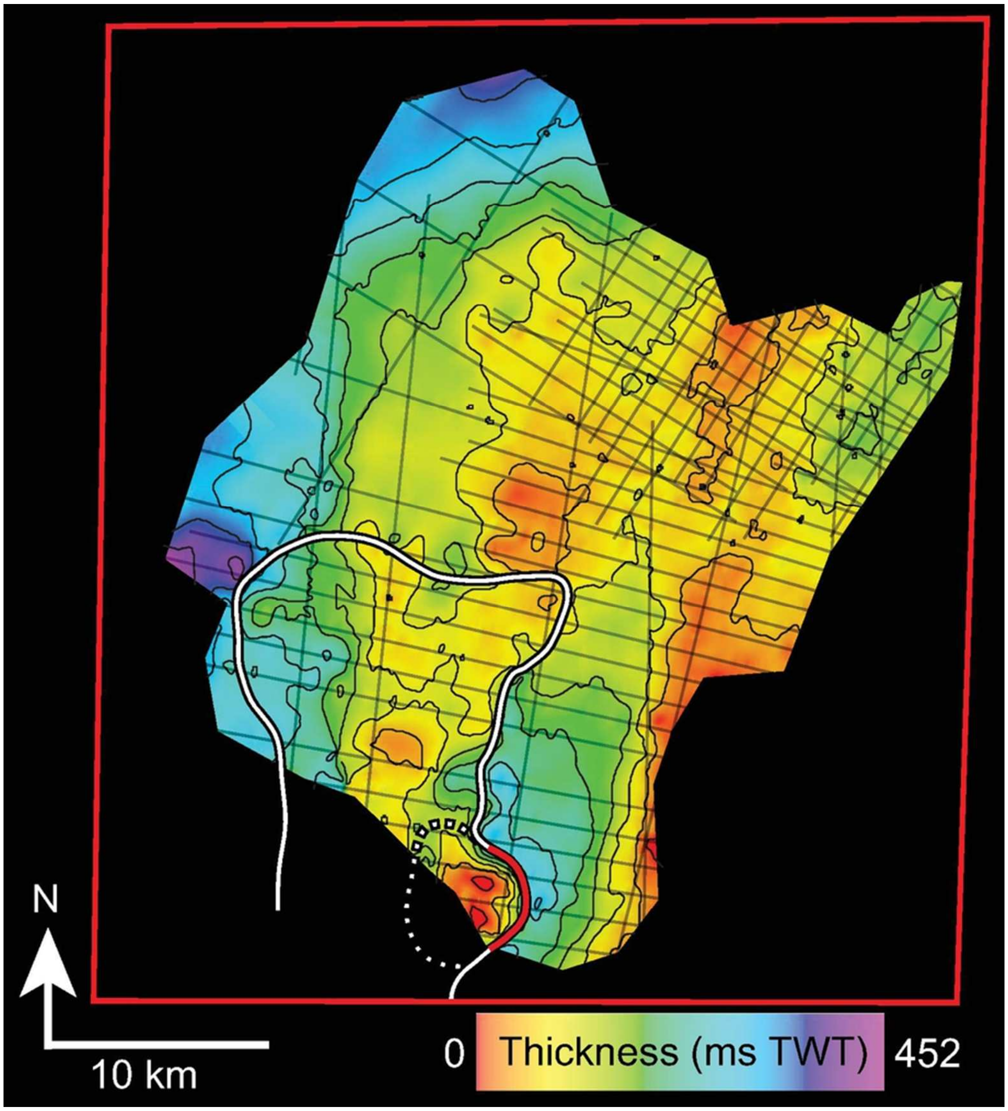

Figure 7: Thickness map of the sedimentary package between horizons C and E. See Figure 2B for location.
Fig. 7
77x85mm (300 x 300 DPI)

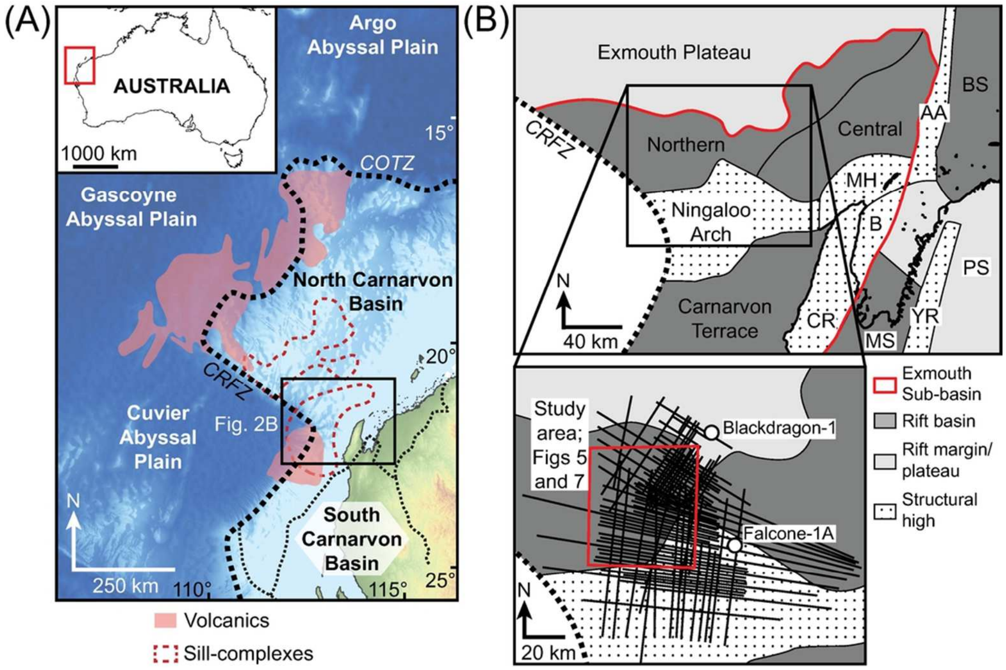

Figure 2: (A) Overview of the NW Australian margin highlighting the extent of Late Jurassic-to-Early Cretaceous sill-complexes and volcanism. COTZ corresponds to the Continent-Ocean Transition Zone and CRFZ is the Cape Range Fracture Zone. (B) Tectonic elements of the study area and a zoomed in viewing showing the distribution of seismic lines (black lines) used here. AA = Alpha Arch; MH = Macedon High; B = Bundegi Terrace; CR = Cape Range Peninsula; PS = Peedamullah Shelf; YR = Yanrey Ridge; MS = Merlinleigh Sub-basin. The Northern and Central elements of the Exmouth Sub-basin are highlighted. Tectonic element configuration taken from Reeve et al. (2016) and references therein.

Fig. 2

92x61mm (300 x 300 DPI)

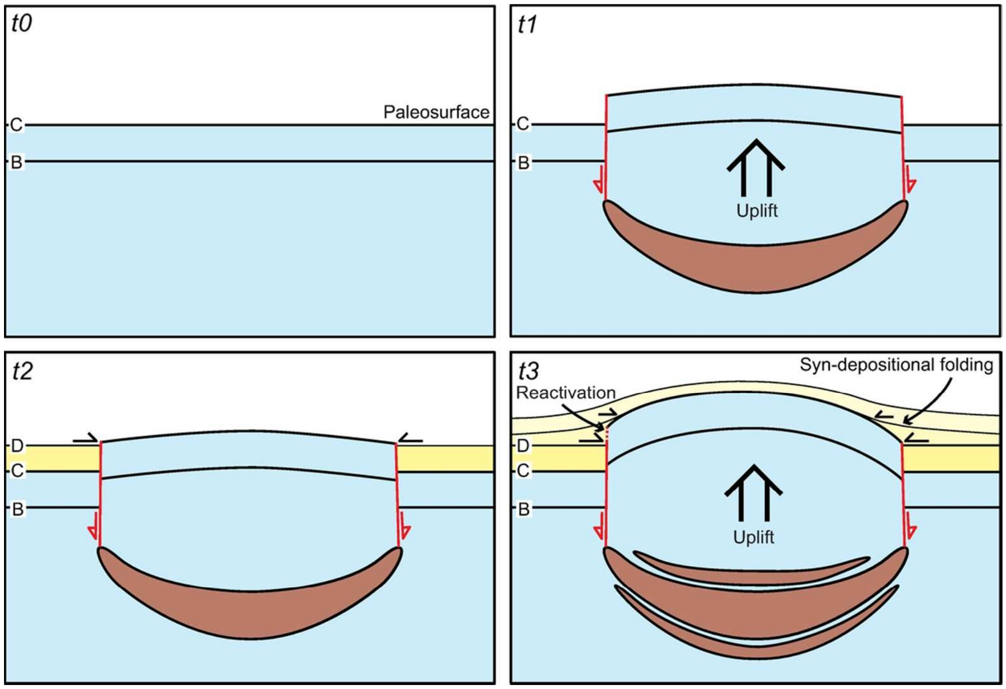

Figure 8: Development of Fold 1, initially via doming and faulting. Emplacement of later, smaller sills can localize deformation within the forced fold, preferentially causing the folding of specific onlapping packages.
Fig. 8
104x71mm (300 x 300 DPI)

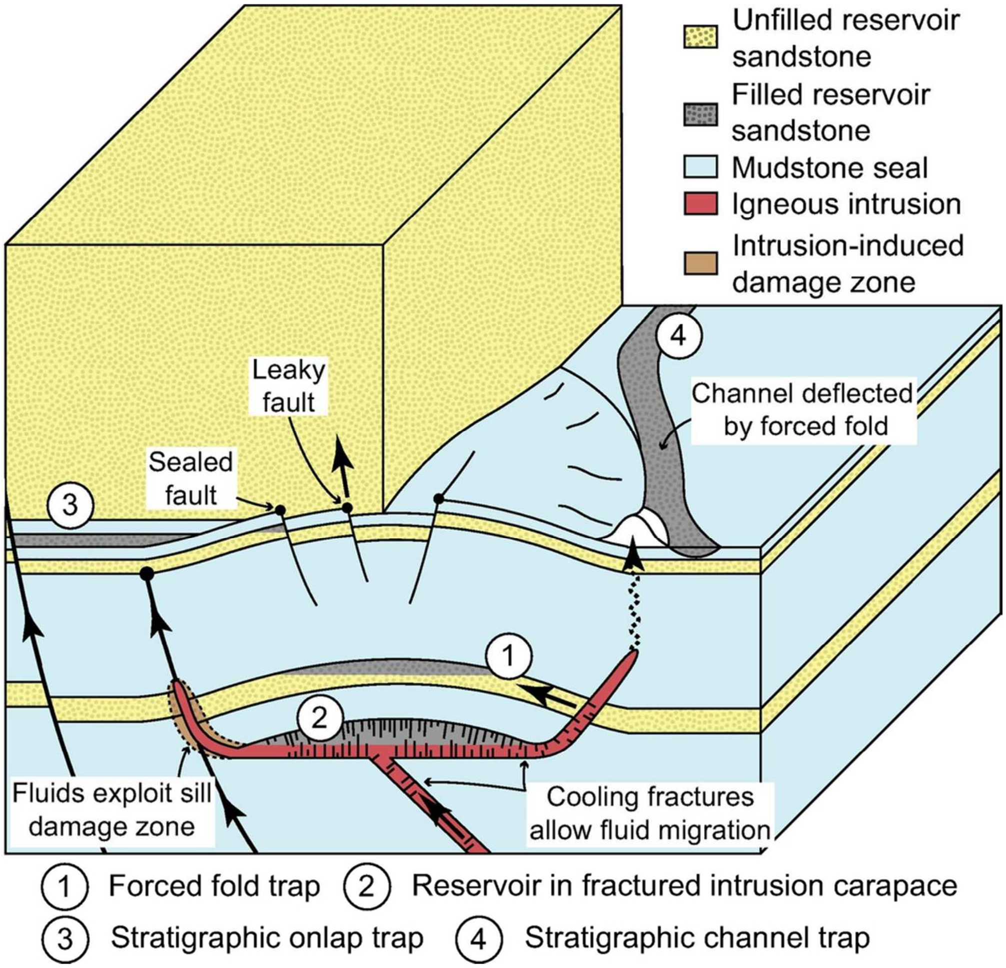

Figure 9: Schematic diagram showing how intrusion-induced forced folds may impact petroleum systems.
See text for details.
Fig. 9
89x85mm (300 x 300 DPI)

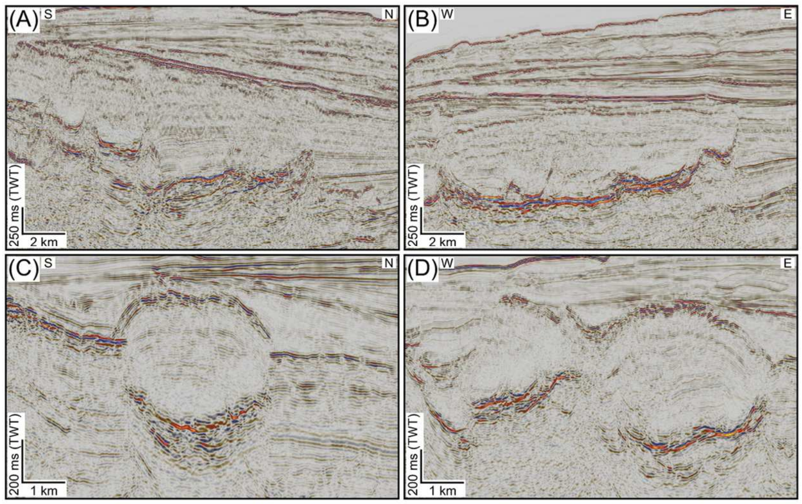

Figure A-1: Uninterpreted detailing the structure of the sills and associated folds 1 and 2. See Figure 6A-D for interpreted sections and Figure 6E for location.
Fig. A-1
123x69mm (300 x 300 DPI)